Resolving structural changes and symmetry lowering in spinel FeCr2S4

Donald M. Evans, Ola G. Grendal, Lilian Prodan, Maximilian Winkler, Noah Winterhalter-Stocker, Philipp Gegenwart, Somnath Ghara, Joachim Deisenhofer, István Kézsmárki, Vladimir Tsurkan

Resolving structural changes and symmetry lowering in spinel FeCr$_2$S$_4$

Donald M. Evans ,[1] Ola G. Grendal ,[2] L. Prodan ,[1,3] Maximilian Winkler,[1] Noah Winterhalter-Stocker,[4]
Philipp Gegenwart ,[4] Somnath Ghara,[1] Joachim Deisenhofer,[1] István Kézsmárki,[1] and V. Tsurkan [1,3,*]

[1]*Experimental Physics 5, Center for Electronic Correlations and Magnetism, Institute of Physics,
University of Augsburg, D-86159 Augsburg, Germany*
[2]*European Synchrotron Radiation Facility, 71 avenue des Martyrs, 38000 Grenoble, France*
[3]*Institute of Applied Physics, MD 2028 Chisinau, R. Moldova*
[4]*Experimental Physics 6, Center for Electronic Correlations and Magnetism, Institute of Physics,
University of Augsburg, D-86159 Augsburg, Germany*

The cubic spinel FeCr$_2$S$_4$ has been receiving immense research interest because of its emergent phases and the interplay of spin, orbital, and lattice degrees of freedom. Despite the intense research, several fundamental questions are yet to be answered, such as the refinement of the crystal structure in the different magnetic and orbital ordered phases. Here, using high-resolution synchrotron powder diffraction on stoichiometric crystals of FeCr$_2$S$_4$ we resolved the long sought-after cubic to tetragonal transition at $\sim$65 K, reducing the lattice symmetry to $I4_1/amd$. With further lowering the temperature, at $\sim$9 K, the crystal structure becomes polar, hence the compound becomes multiferroic—likely reducing the space group to $I4_1md$. The elucidation of the lattice symmetry throughout different phases of FeCr$_2$S$_4$ provides a basis for the understanding this enigmatic system and also highlights the importance of structural deformation in correlated materials.

I. INTRODUCTION

Over the last 50 years FeCr$_2$S$_4$, a prominent member of the large cubic chalcogenide spinel family, has been reported to exhibit a rich variety of physical phenomena emerging from the complex interplay of charge, spin, orbital, and structural degrees of freedom. These fascinating phenomena include colossal magnetoresistance [1], half metallicity [2], dynamic and static Jahn-Teller effects [3–7], Coulomb-enhanced spin-orbit interaction [8,9], topological anomalous Hall effect [10], multiferroicity [11,12], and magnetostructural transformations [11,13–16]. However, this compound is highly sensitive to subtle changes in stoichiometry, which makes it difficult to establish the microscopic origins behind these phenomena. Specifically, the changes in stoichiometry cause notable alteration to the magnetic and structural properties [17,18]. For instance, the phase transition at $\sim$9 K, recently documented in the magnetization and specific heat also in FeCr$_2$S$_4$ single crystals [15], is only observed in samples with stoichiometry close to ideal value. Indeed, it can be fully suppressed by defects or site interchange of the cations of the order of 1–2% [17,19–21], which can rarely be excluded during the synthesis and crystal growth of spinel-type materials.

Despite the challenges of this intriguing system, magnetic properties in the low-field phases are believed to be well characterized. The stoichiometric FeCr$_2$S$_4$ is reported to order ferrimagnetically at $T_C \sim 165$ K [15,22]. Below T_C down to $T_m \sim 65$ K, the magnetic structure is collinear with an antiferromagnetic arrangement of spins of the tetrahedrally coordinated Fe^{2+} and octahedrally coordinated Cr^{3+} ions [11,23]. Below T_m, the collinear spin structure transforms into an incommensurate one, which remains the stable spin configuration down to the lowest temperature [24]. The temperature T_m has previously been associated with local structural distortions attributed to dynamic Jahn-Teller (JT) correlations [22]. At $T_{OO} \sim 9$ K, there was an unconventional first-order magnetostructural transition reported, which is associated with a peak in the specific heat and $\sim$20% reduction in the magnetic anisotropy [13,15,22].

Behind these well-established magnetic transitions, the low-temperature space group symmetry has remained an enigma over the years. Some indications for the deviations from the cubic $Fd3m$ symmetry, structural distortions, and structural transition at low temperatures have been provided by earlier Mössbauer measurements [4–7,25]. Additional hints for the structural anomaly at around T_m came out from the ac susceptibility [26] and transmission-electron microscopy [27] studies. Note that previous x-ray and neutron powder diffraction studies have not detected any structural anomaly at low temperatures anticipated for the JT effect [23,28–30]. Even high-resolution synchrotron x-ray diffraction on stoichiometric polycrystals could not resolve the reduction of the symmetry with respect to the cubic structure, noticing however, the broadening of the diffraction peaks below T_m, which reaches a maximum at T_{OO} [22]. Further insights have been provided by recent reports on the appearance of the multiferroic polar state below T_{OO} [11,12] and on optical properties in the THz and FIR frequency range [14,31], which evidenced the reduction of the lattice symmetry below

T_m and T_{OO}, although the symmetry of the low-temperature phase remained unresolved.

It is necessary to note that the problem of structural transformations in transition-metal (TM) spinels containing JT active ions at the tetrahedral *A* sites is a matter of many years studies and discussion since 1960s [32,33]. In ferrimagnetic TM oxide spinels, for example, in $Me\mathrm{Cr_2O_4}$ (Me = Fe, Ni, and Cu), the transition from the cubic $Fd3m$ to the tetragonal $I4_1/amd$ structure, related to JT ordering, was found at temperatures far above the temperature of their long-range spin ordering. Recent studies revealed a further reduction of the structural symmetry from the tetragonal to orthorhombic $Fddd$ symmetry, which is coupled either to the onset of the ferrimagnetic order or to change of the spin configuration, e.g., from collinear to noncollinear, or ordering of the antiferromagnetic component of the magnetic moment [34–37]. In the *A*-site cubic TM chalcogenide spinels, JT ordering was reported only for $\mathrm{FeCr_2S_4}$. In $\mathrm{FeCr_2S_4}$, the JT energy is much lower than in the TM oxides and the respective JT distortions are anticipated at a significantly lower level. The structural changes associated with the JT ordering here develop on a background of distortions related to already established long-range ferrimagnetic order due to significant spin-lattice coupling [14]. Together with the above mentioned nonstoichiometry problem, this makes the observation of the symmetry-lowering transition extremely challenging for $\mathrm{FeCr_2S_4}$.

In this paper, based on the results of high-resolution synchrotron x-ray diffraction study performed on stoichiometric $\mathrm{FeCr_2S_4}$ we establish that the low-temperature structure is described by a polar subgroup of the tetragonal $I4_1/amd$ space group. The symmetry lowering from the cubic $Fd3m$ to the tetragonal $I4_1/amd$ is resolved below $T_m \sim 65$ K. We correlate our structural data with the data of the thermal expansion, electronic, magnetic, and heat capacity measurements. The pyrocurrent measurements allow us to conclude that below T_{OO} the symmetry is further reduced to a polar subgroup of $I4_1/amd$. This holistic view of the phase transitions allows us to analyze the key traits for each transition, to offer an understanding of the crystal as a whole, crucial for future experimental and theoretical work.

II. EXPERIMENTAL METHODS

All experiments presented here were performed on stoichiometric single crystals grown by the chemical transport reactions as described in Ref. [14].

A. X-ray powder diffraction

To prepare a sample for the x-ray diffraction experiment, single crystals of $\mathrm{FeCr_2S_4}$ were selected, based on having high quality growth faces, and ground to a powder. The powder was annealed in evacuated quartz ampoule at $400\,^{\circ}\mathrm{C}$ for two weeks, to remove any stress eventually induced by the grinding, before being stored and transported in vacuum conditions. The powder was filled into a 0.5-mm boron-silicate glass capillary. High-resolution powder x-ray diffraction (XRD) data were collected in transmission geometry on the high-resolution setup at the ID22 beamline, at

European Synchrotron Radiation Facility (ESRF), Grenoble, France [38,39]. The wavelength was calibrated using silicon (NIST, 640c) to 0.354217 Å (35 keV). Data were collected at 4, 7, 9, 15, 35, 60, 80, 100, 140, 165, and 190 K with the temperature being controlled with a liquid Helium cooled cryostat, and additional data were collected at ambient conditions (295 K) outside the cryostat. To reduce the effect of beam heating, the capillary was kept open at one end and exposed to the helium-flow atmosphere; in addition, the beam was attenuated for the experiments performed at 90 K and below. We note that the temperature reported is measured on the helium flow, and so the actual sample temperature is expected to be slightly higher than the stated value, due to heating from the beam.

Rietveld refinements and space group and lattice parameter determination of the low temperature phase were done using TOPAS (version 7). The most probable candidate structure for the low-temperature phase was found by combing the result from the diffraction pattern indexing and group-subgroup relations from *Bilbao Crystallographic* server [40].

B. Resistivity and polarization

A single crystal with well-defined {111} facets was selected from the same batch used in the powder diffraction studies, polished down to thin slab parallel the (111) plane of the cubic setting. For both resistivity and pyrocurrent measurements, the electrical contacts were applied on these (111) faces with silver paint and gold wires. The electrical resistivity experiments were performed in the frame of conventional four-probe method in the temperature range from 10 K to 300 K using the resistivity option of the commercial Quantum Design physical property measurement system (PPMS). The pyrocurrent measurements were carried out in a capacitor-contact geometry using Oxford Helium flow cryostat together with the Keysight B2987A electrometer. This enables measurements between 300 and 2 K with the application of a magnetic field up to 14 T. The pyrocurrent data were obtained after cooling the sample from 20 K to 2 K in the presence of electric ($E_p = 1$ kV/cm) and magnetic ($\mu_0 H_p = 4$ T) poling fields. The poling fields were applied parallel to the crystallographic $\langle 111 \rangle$ direction of the cubic setting. The pyroelectric current was measured in constant magnetic fields after switching off the electric field and keeping the sample short-circuited for at least 2 min while heating up with a constant rate of 4 K/min. The electric polarization was obtained by integration of the pyrocurrent with respect to time.

C. Thermal expansion

Thermal expansion was measured with the aid of a compact ultrahigh-resolution capacitive dilatometer [41] in the Quantum Design physical property measurement system (PPMS). A single crystal with well-defined {111} facets was oriented and polished to prepare a plane parallel sample with $\langle 100 \rangle$ orientation. For this measurement a sample with a thickness of 0.33 mm was used. The cell background was subtracted as it is described in Ref. [42]. For that purpose, a sample of pure copper with the same thickness as the sample was measured. To ensure good thermalization, the thermal
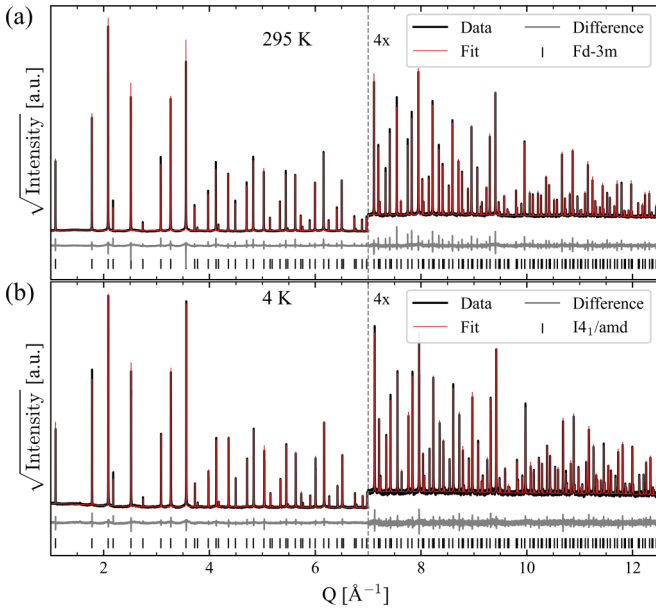
FIG. 1. (a) Room temperature and (b) 4 K synchrotron high-resolution x-ray powder diffraction spectra of $FeCr_2S_4$. Rietveld refinement of spectra at 4 K with $I4_1/amd$ space group. $R_{wp} = 12.62\%$, $R_{exp} = 8.27\%$, $GOF = 1.53$.

expansion was measured from 2 to 200 K with a sweeping rate of 0.3 K/min. Several up and down sweeps were measured to verify the measured behavior.

D. Magnetization and specific heat

The magnetic properties have been studied on single-crystalline samples using a SQUID magnetometer (Quantum Design MPMS 3) in static fields applied parallel to the cubic $\langle 111 \rangle$ axis. The specific heat was measured in the commercial Quantum Design physical property measurement system (PPMS).

III. EXPERIMENTAL RESULTS

X-ray powder diffraction

We start by confirming the room-temperature structure using the high-resolution diffraction data presented in Fig. 1(a). The recorded data (black lines) are fitted well (red lines) with the expected room temperature space group $Fd3m$, no. 227, a = 9.99816 Å, Z = 8. The difference between fitted and expected values are plotted as grey lines and the expected peak positions are given by the black ticks. These data show no evidence for a secondary phase or other impurities. The data collected at base temperature, 4 K, are presented in Fig. 1(b) and the indexing show a good fit with the tetragonal space group $I4_1/amd$ (no. 141, a = 7.0577 Å, c = 9.97793 Å, Z = 4). Cubic, tetragonal, orthorhombic, and hexagonal space groups were also searched for when indexing, however, no cubic or hexagonal space group were found to match all the observed peaks. Also, none of the orthorhombic space groups, including $Fddd$, gave any significant improvement of the refinements over the proposed tetragonal space group. Taking into consideration that the direct transition from the cubic to
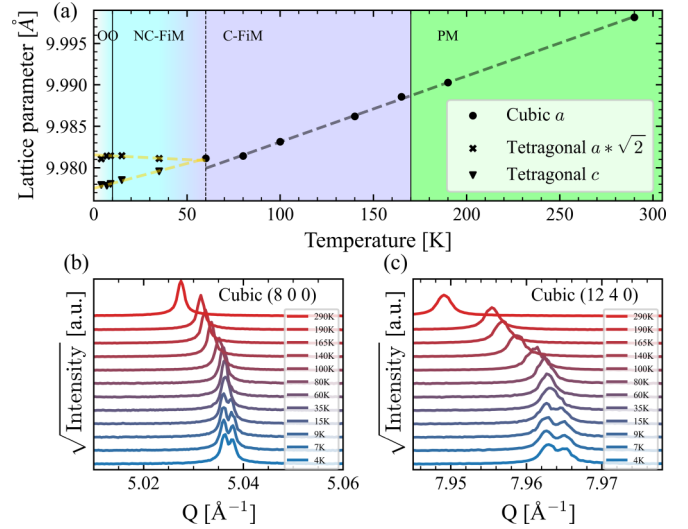

FIG. 2. (a) Temperature dependence of the lattice parameters. Vertical grey dotted line shows separation between the use of the cubic and tetragonal space group for the Rietveld refinements. PM, C-FiM, NC-FiM, and OO mark respectively, cubic paramagnetic, pseudocubic collinear ferrimagnetic, tetragonal noncollinear ferrimagnetic, and tetragonal orbitally ordered multiferroic phases. (b) Temperature dependence of the cubic (8 0 0) peak. (c) Temperature dependence of the (12 4 0) peak. Both (b) and (c) show a clear splitting at 15 K and below, and a broadening already below 60 K.

orthorhombic symmetry assumes a first-order structural transformation, in contradiction to the experimental observation, we therefore exclude the orthorhombic $Fddd$ symmetry for the structure below T_m.

IV. DISCUSSION

For the sake of clarity, we discuss the three transitions individually: (i) the high-temperature para-to-ferrimagnetic transition at $T_C \sim 165$ K; (ii) the transition at $T_m \sim 65$ K that is associated with structural distortion and spin reorientation, and (iii) further anomalies below 20 K, including the transition at T_{OO}.

Having successfully identified the high- and low-temperature structures, we collected additional spectra to find the structural transition temperature and see if any of the other known transitions affect the lattice parameters. This is best illustrated by the temperature dependency of the lattice parameters, presented in Fig. 2(a). Note the same fitting approach was used at all temperatures. Figure 2(a) shows a nearly linear thermal contraction of the lattice parameter a (see fitted grey line) down to 80–60 K, below which the rate of thermal contraction changes. The grey-dashed line in Fig. 2(a) terminates at low temperatures, where the fitting was changed from cubic to tetragonal structure, as discussed and justified below. Interestingly, the tetragonality (the difference between a and c lattice parameters) shows a monotonous increase until 7 K, below which it reduces.

Our primary interest is in the onset of the tetragonal distortions, i.e., when the difference in the a and c lattice parameters can be resolved. An analysis of the individual peaks in Figs. 2(b) and 2(c), shows an apparent shoulder at 35 K in
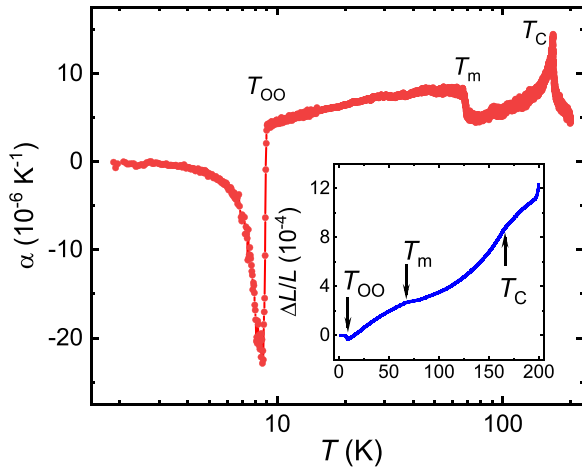
FIG. 3. Temperature dependence of the thermal expansion coefficient α of single crystalline FeCr$_2$S$_4$. Inset: Temperature dependence of the normalized sample length $\Delta L/L$. Arrows mark the phase transition temperatures.

the (12 4 0) reflection, and a clear splitting in the (8 0 0) and (12 4 0) reflections in all diffraction patterns collected at and below 15 K. Such a resolvable peak splitting diagnostically establishes that the symmetry has been reduced from cubic for these temperatures. Although at temperatures above 15 K a clear splitting cannot be resolved instrumentally, the structural distortion is already manifested in a broadening of these peaks. One possible way to estimate the actual temperature when the material loses cubic symmetry is by extrapolation of the temperature dependency of the low-symmetry lattice parameters. Here we only note that we have treated the 35 K data as tetragonal based on: (i) significant peak broadening compared with data at 60 K, and (ii) extrapolated thermal contraction data (see Sec. IV).

A. Thermal expansion

In addition to the synchrotron powder diffraction, we performed thermal expansion experiments to characterize the macroscopic behavior of the sample. Figure 3 shows the temperature dependence of the thermal expansion coefficient α calculated from measurements of the change in the sample length on heating shown in the inset of this figure. This dataset has several prominent features: a clear peak marking $T_C \sim$ 165 K, a step like change at $T_m \sim 65$ K, and a lambda-type anomaly at $T_{OO} \sim 9$ K, where α changes the sign from positive to negative.

B. Resistivity and polarization

To understand how the structural properties couple to the electronic orders, we measured resistivity and electric polarization on single crystals from the same batch. The data are presented in Figs. 4(a) and 4(b), respectively. The resistivity data show that the sample is a semiconductor at room temperature [$\rho(300K) \sim 80\,\Omega$ cm] and becomes highly insulating at low temperature, [$\rho(16K) \sim 1.5$ x $10^6\,\Omega$ cm]. There is a hump in the resistivity at $\sim$170 K, slightly above the onset of ferrimagnetic order at T_C.
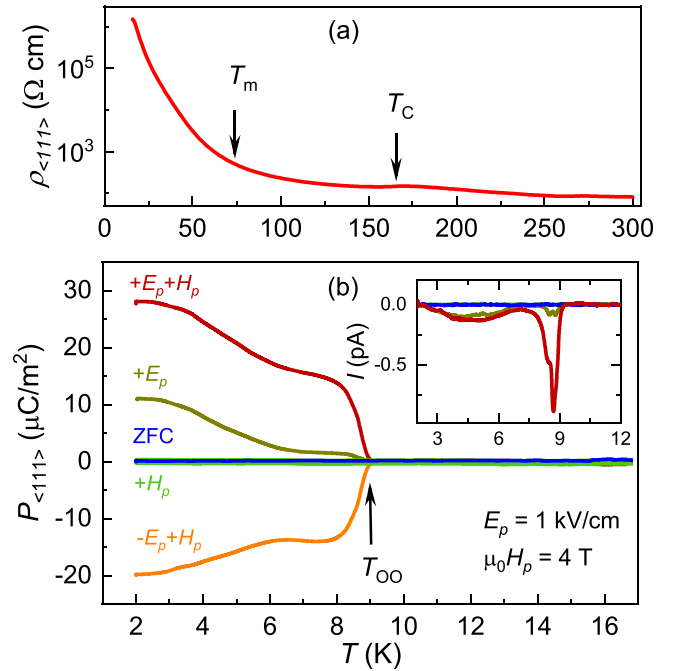

FIG. 4. (a) Temperature-dependent resistivity measurements. (b) Polarization P vs T. The different colors show the different applied fields with the direction of the polarization depending on the sign of the applied electric field, consistent with ferroelectricity. Inset: Pyrocurrent I vs T taken on cooling with the fields labeled in (b).

The current x-ray experiments provide the resolution of the lattice parameters but powder diffraction cannot resolve the difference between polar and nonpolar space groups. To test for polar phases, we measured electric polarization below 20 K, where the material is insulating enough for such studies. Figure 4(b) shows the temperature dependence of the polarization, calculated by integration of the pyrocurrent data measured under different poling conditions. Interestingly, there is no anomaly in the polarization data if the sample is cooled after poling in a magnetic field but in the absence of a poling electric field. After poling the crystal in the electric field only, a small polarization $P \sim 2\,\mu$C m^{-2} appears below $T_{OO} \sim 9$ K, whose sign depends on the direction of the applied poling voltage (not shown for clarity). This indicates the sample is ferroelectric, as the sign of the polarization is switchable through the phase transition. Importantly, the polarization at the transition can be significantly increased to $\sim$15 μC m^{-2} with additional presence of a magnetic field, suggesting either that magnetoelectric coupling is important, or that the electric field alone is not enough to orient the magnetostructural domains. Note that the sign of the polarization is independent of the sign of the applied magnetic field, implying an even coupling term. The pyrocurrent curves in the inset of Fig. 4(b) also reveal a second broad feature starting below $\sim$6 K, the origin of which is unclear. We cannot rule out that it is related to thermally stimulated discharge currents, which lead to additional polarization of $\sim$13 μC m^{-2}, resulting from the integration of pyrocurrent over a wide-temperature range below 6 K.
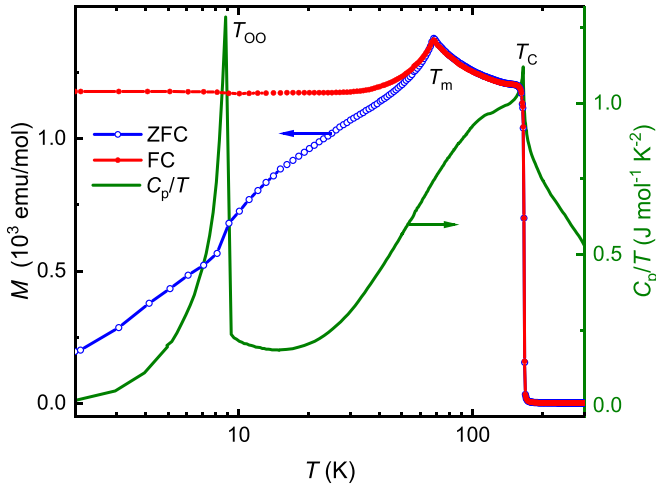
FIG. 5. ZFC and FC magnetizations measured in a field of 0.01 T (left axis) and specific heat in representation C_p/T in zero field (right axis) collected on the same sample. Both data sets show a step like anomaly at the onset of the magnetic ordering at $T_C \sim 165$ K. The magnetic data have an additional peak at $T_m \sim 65$ K, while a clear peak at $T_{OO} \sim 9$ K in the specific heat is only slightly pronounced in the magnetization.

C. Para-to-ferrimagnetic transition

This transition is clearly manifested in thermodynamic quantities, namely the magnetization and the specific heat (see Fig. 5). There is also a broad peak in the resistivity data in Fig. 4(a), originating from the scattering of the conducting electrons by fluctuations of the magnetic moments that are maximal at T_C, giving rise to colossal magnetoresistance [1]. There is no evidence of an anomaly in our x-ray data, with the lattice parameters apparently changing linearly with temperature across this transition, see Fig. 2(a). At the same time, the presence of a clear peak in the thermal expansion coefficient at T_C, Fig 3, which is associated with exchange striction, suggests that the structural changes do take place although the deviation from the cubic symmetry, which is a necessary consequence of the onset of the long-range ferrimagnetic order, cannot be resolved even in our high-resolution x-ray study. For this reason, we refer to the phase between $T_m < T < T_C$ as a pseudocubic ferrimagnetic state.

D. Cubic-to-tetragonal transition

From our synchrotron data we can conclude that the material is clearly tetragonal at and below 15 K. The precise determination of the onset of the cubic-to-tetragonal transition is compromised by the resolution of our experiment. While a broadening of specific cubic Bragg peaks is observed below 60 K, their splitting to two peaks is well resolved only at and below 15 K. Fortuitously, when refining the structure below 65 K using the tetragonal space group $I4_1/amd$, the obtained a and c lattice parameters coincide at ~ 65 K and deviate linearly below this temperature as depicted by the yellow dashed lines in Fig. 2(a). This approach is supported and substantiated by the thermal expansion coefficient of Fig. 3, which shows the expected change in trend across $T_m \sim 65$ K. The presence of a structural phase transition can also explain
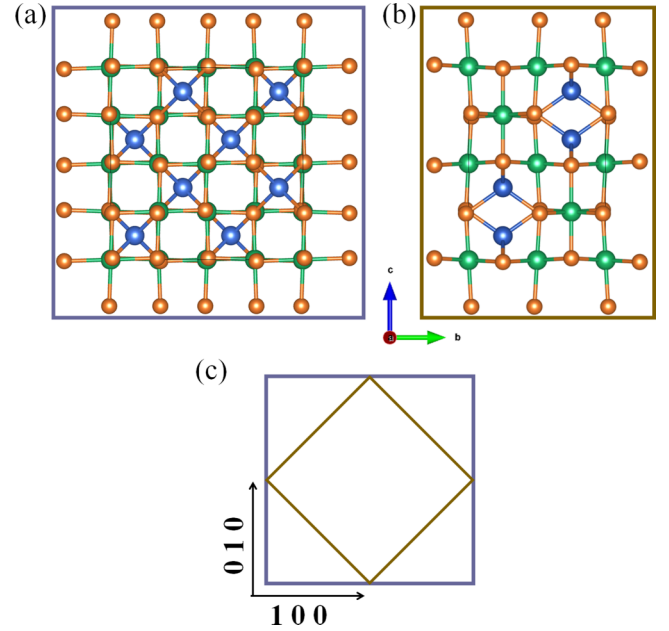

FIG. 6. High-temperature cubic $Fd3m$ unit cell. (b) Low-temperature tetragonal $I4_1/amd$ unit cell. In both (a) and (b) the blue atoms are Fe, the green atoms are Cr, and the gold atoms are S. (c) Schematic of the redefined unit cell across the structural transformation. Panels (a) and (b) are made using VESTA [43].

the divergence of the ZFC and FC magnetizations in Fig. 5 and implies a simultaneous change in the magnetic structure. This is naturally expected, since the cubic to tetragonal distortion activates the axial magnetic anisotropy in this compound.

In contrast, neither the resistivity nor the specific heat shows pronounced anomalies at this temperature. This implies that the changes in the phonon energy and the scattering rate of the itinerant electrons are subtle at this magnetostructural transition. Our synchrotron data indicate that the symmetry of the unit cell changes from $Fd3m$ to $I4_1/amd$ through this transition. These structures are schematically depicted in Figs. 6(a) and 6(b), respectively. Both of these unit cells are viewed down the room temperature a axis. The a and b axes in the low-temperature tetragonal structure are rotated by 45° with respect to the [100] and [010] cubic axes, as schematically shown in Fig. 6(c).

E. Onset of polar order

While powder x-ray diffraction in the present case does not permit the distinction of polar and nonpolar tetragonal space groups, the appearance of a peak in pyrocurrent at T_{OO} provides clear evidence for the onset of a ferroelectric phase as can be followed in Fig. 4(b). This is associated with a step-wise change in the thermal expansion coefficient, and a lambda-like anomaly in the specific heat. The fact that the magnitude of the pyrocurrent can be enhanced with a magnetic field, applied in addition to an electric field, strongly suggests this phase is a multiferroic phase.

Curiously, despite the multiferroic nature of this phase, the application of a magnetic field on its own is not able to establish a net polar moment. In contrast, an electric field

leads to finite polarization. Surprisingly, the combination of electric and magnetic field can substantially increase the ferroelectric polarization. This may be understood in the following scenario. Electric field applied along any of the cubic $\langle 100 \rangle$ axes, favours and increases the population of the tetragonal structural domain states with c axis coaligned with the field and, at the same time, it also favours the domain state with polarization along the electric field with respect to the domain state with opposite polarization. However, not even the strongest electric fields applied in this study can create a structural mono-domain state and saturate the polarization. The action of the magnetic field, applied along any of the cubic $\langle 100 \rangle$ axes, is different: it also favours the tetragonal structural domain states with c axis coaligned with the field, but would not switch their polar moments. For this reason, electric and magnetic fields act cooperatively and lead to increased polarization.

Based on our observations we can make some inferences about the symmetry of the ground state. Our synchrotron study confirms that the symmetry in the state below T_{OO} is tetragonal. While the synchrotron study could not distinguish between the centrosymmetric and polar tetragonal structures, as follows from the Friedel's law, the observation of finite electric polarization below T_{OO} indicates that the crystal structure must be polar and thus, the symmetry must be further reduced from $I4_1/amd$. The tetragonal polar subgroup of $I4_1/amd$ are $I4_1$ and $I4_1md$. We found that refining x-ray data with the $I4_1$ space group leaves the atoms in general Wyckoff positions close to special Wyckoff positions in higher symmetry $I4_1md$ and the R values are effectively unchanged. This suggests that the higher symmetry is sufficient to describe the structure. In addition, extra reflections, e.g., (334), are allowed for $I4_1$ and are absent in $I4_1md$, and as our data has no intensity at these (hkl) positions, it suggests that $I4_1md$ is the most likely space group. The tetragonal magnetic point groups, which allow spontaneous electric polarization are 4, $4'$, $4mm$, $4'mm'$, and $4m'm'$. Since the present compound exhibits a finite ferromagnetic component along the tetragonal axis, 4 and $4m'm'$ are the most probable magnetic point groups.

V. CONCLUSIONS

In this paper, we investigated the sequence of the phase transitions within spinel $FeCr_2S_4$ using structural, electronic, thermodynamic, and magnetic measurements. Using high-resolution synchrotron data, we could confirm the previously assumed tetragonal phase at low temperatures, below $T_m \sim$ 65 K. Above this temperature, no deviation of the cubic crystal structure was resolved, although the material becomes ferrimagnetic already below $T_C \sim 165$ K. Therefore, we refer to the phase between 65–165 K as a pseudocubic ferrimagnet. While no further lowering of the symmetry could be traced in our x-ray data down to 4 K, our pyroelectric measurements reveal a transition from the nonpolar tetragonal state to a polar tetragonal state at $T_{OO} \sim 9$ K, likely reducing the space group to $I4_1md$, with the possible magnetic point group symmetries 4 or $4m'm'$. As such, we have clarified several long-standing questions in this enigmatic compound, but more work, potentially including direct imaging of the microstructure, is required.

[1] A. P. Ramirez, R. J. Cava, and J. Krajewski, Colossal magnetoresistance in Cr-based chalcogenide spinels, Nature (London) **386**, 156 (1997).

[2] M. S. Park, S. K. Kwon, S. J. Youn, and B. I. Min, Half-metallic electronic structures of giant magnetoresistive spinels: $Fe_{1-x}Cu_xCr_2S_4$ ($x = 0.0, 0.5, 1.0$), Phys. Rev. B **59**, 10018 (1999).

[3] L. F. Feiner, Unified description of the cooperative Jahn-Teller effect in $FeCr_2S_4$ and the impurity Jahn-Teller effect in $CoCr_2S_4$:Fe^{2+}, J. Phys. C: Solid State Phys. **15**, 1515 (1982).

[4] M. Eibschutz, S. Shtrikman, and Y. Tenenbaum, Magnetically induced electric field gradient in tetrahedral divalent iron: $FeCr_2S_4$, Phys. Lett. A **24**, 563 (1967).

[5] M. R. Spender and A. H. Morrish, A low-temperature transition in $FeCr_2S_4$, Solid State Commun. **11**, 1417 (1972).

[6] L. Brossard, J. L. Dormann, L. Goldstein, P. Gibart, and P. Renaudin, Second-order phase transition in $FeCr_2S_4$ investigated by Mössbauer spectroscopy: An example of orbital para-to-ferromagnetism transition, Phys. Rev. B **20**, 2933 (1979).

[7] A. M. van Diepen and R. P. van Stapele, Ordered local distortions in cubic $FeCr_2S_4$, Solid State Commun. **13**, 1651 (1973).

[8] S. Sarkar, M. De Raychaudhury, I. Dasgupta, and T. Saha-Dasgupta, Electronic structure of $FeCr_2S_4$: Evidence of Coulomb enhanced spin-orbit splitting, Phys. Rev. B **80**, 201101(R) (2009).

[9] S. Sarkar, T. Maitra, Roser Valentí, and T. Saha-Dasgupta, Comparative study of $FeCr_2S_4$ and $FeSc_2S_4$: Spinels with orbitally active A site, Phys. Rev. B **82**, 041105(R) (2010).

[10] K. Ohgushi, S. Miyasaka, and Y. Tokura, Anisotropic anomalous Hall effect of topological origin in carrier-doped $FeCr_2S_4$, J. Phys. Soc. Jpn. **75**, 13710 (2006).

[11] J. Bertinshaw, C. Ulrich, A. Günther, F. Schrettle, M. Wohlauer, S. Krohns, M. Reehuis, A. J. Studer, M. Avdeev, D. V. Quach *et al.*, $FeCr_2S_4$ in magnetic fields: Possible evidence for a multiferroic ground state, Sci. Rep. **4**, 6079 (2014).

[12] L. Lin, H. X. Zhu, X. M. Jiang, K. F. Wang, S. Dong, Z. B. Yan, Z. R. Yang, J. G. Wan, and J. M. Liu, Coupled ferroelectric polarization and magnetization in spinel $FeCr_2S_4$, Sci. Rep. **4**, 6530 (2014).

[13] V. Felea, S. Yasin, A. Günther, J. Deisenhofer, H.-A. Krug von Nidda, E.-W. Scheidt, D. V. Quach, J. R. Groza, S. Zherlitsyn, V. Tsurkan *et al.*, Ultrasound study of $FeCr_2S_4$ in high magnetic fields, J. Phys: Condens. Matter **26**, 486001 (2014).

[14] J. Deisenhofer, F. Mayr, M. Schmidt, A. Loidl, and V. Tsurkan, Infrared-active phonons in the ferrimagnetic and multiferroic phases of $FeCr_2S_4$: Evidence for structural distortions, Phys. Rev. B **100**, 144428 (2019).

[15] L. Prodan, S. Yasin, A. Jesche, J. Deisenhofer, H. A. K. von Nidda, F. Mayr, S. Zherlitsyn, J. Wosnitza, A. Loidl, and V. Tsurkan, Unusual field-induced spin reorientation in $FeCr_2S_4$: Field tuning of the Jahn-Teller state, Phys. Rev. B **104**, L020410 (2021).

[16] V. Tsurkan, H.-A. Krug von Nidda, J. Deisenhofer, P. Lunkenheimer, and A. Loidl, On the complexity of spinels: Magnetic, electronic, and polar ground states, Phys. Rep. **926**, 1 (2021).

[17] F. K. Lotgering, A. M. van Diepen, and J. F. Olijhoek, Mössbauer spectra of iron-chromium sulfospinels with varying metal ratio, Solid State Commun. **17**, 1149 (1975).

[18] P. Gibart, L. Golstein, and L. Brossard, Non stoichiometry in $FeCr_2S_4$, J. Magn. Magn. Mater. **3**, 109 (1976).

[19] V. Tsurkan, V. Fritsch, J. Hemberger, H.-A. Krug von Nidda, D. Samusi, S. Körner, E.-W. Scheidt, S. Horn, R. Tidecks, and A. Loidl, Orbital fluctuations and orbital order in $FeCr_2S_4$, J. Phys. Chem. Solids **66**, 2036 (2005).

[20] V. Tsurkan, H.-A. Krug von Nidda, A. Krimmel, P. Lunkenheimer, J. Hemberger, T. Rudolf, and A. Loidl, Ternary magnetic semiconductors: Recent developments in physics and technology, Phys. Stat. Sol. A **206**, 1082 (2009).

[21] R. Tong, Z. R. Yang, S. Shen, X. B. Zhu, Y. P. Sun, L. Li, S. L. Zhang, L. Pi, and Y. H. Zhang, Disorder-induced orbital glass state in $FeCr_2S_4$, Europhys. Lett. **89**, 57002 (2010).

[22] V. Tsurkan, O. Zaharko, F. Schrettle, C. Kant, J. Deisenhofer, H.-A. Krug von Nidda, V. Felea, P. Lemmens, J. R. Groza, D. V. Quach, F. Gozzo, and A. Loidl, Structural anomalies and the orbital ground state in $FeCr_2S_4$, Phys. Rev. B **81**, 184426 (2010).

[23] G. Shirane, D. E. Cox, and S. J. Pickart, Magnetic structures in $FeCr_2S_4$ and $FeCr_2O_4$, J. Appl. Phys. **35**, 954 (1964).

[24] G. M. Kalvius, A. Krimmel, O. Hartmann, R. Wäppling, F. E. Wagner, F. J. Litterst, V. Tsurkan, and A. Loidl, Low temperature incommensurately modulated and noncollinear spin structure in $FeCr_2S_4$, J. Phys.: Condens. Matter **22**, 052205 (2010).

[25] M. R. Spender and A. H. Morrish, Mössbauer study of the ferrimagnetic spinel $FeCr_2S_4$, Canad. J. Phys. **50**, 1125 (1972).

[26] V. Tsurkan, J. Hemberger, M. Klemm, S. Klimm, A. Loidl, S. Horn, and R. Tidecks, Ac susceptibility studies of ferrimagnetic $FeCr_2S_4$ single crystals, J. Appl. Phys. **90**, 4639 (2001).

[27] M. Mertinat, V. Tsurkan, D. Samusi, R. Tidecks, and F. Haider, Low temperature structural transition in $FeCr_2S_4$, Phys. Rev. B **71**, 100408(R) (2005).

[28] C. Broquetas Colominas, R. Ballestracci, and G. Roult, Étude par diffraction neutronique du spinelle $FeCr_2S_4$, J. Phys. France **25**, 526 (1964).

[29] S. J. Kim, W. C. Kim, and C. S. Kim, Neutron diffraction and magnetotransport properties in sulphur spinel, J. Magn. Magn. Mater. **242**, 201 (2002).

[30] L. Lo Presti, D. Invernizzi, R. Soave, and R. Destro, Looking for structural phase transitions in the colossal magnetoresistive thiospinel $FeCr_2S_4$ by a multi-temperature single-crystal X-ray diffraction study, Chem. Phys. Lett. **416**, 28 (2005).

[31] A. Strinić, S. Reschke, K. V. Vasin, M. Schmidt, A Loidl, V. Tsurkan, M. V. Eremin, and J. Deisenhofer, Magnetoelectric properties and low-energy excitations of multiferroic $FeCr_2S_4$, Phys. Rev. B **102**, 134409 (2020).

[32] J. D. Dunitz and L. E. Orgel, Electronic properties of transition-metal oxides-1. Distortions from cubic symmetry, J. Phys. Chem. Solids **3**, 20 (1957).

[33] J. B. Goodenough, Jahn-Teller distortions induces by tetrahedral-site Fe^{2+} ions, J. Phys. Chem. Solids **25**, 151 (1964).

[34] H. Ishibashi and T. Yasumi, Structural transition of spinel compound $NiCr_2O_4$ at ferrimagnetic transition temperature, J. Magn. Magn. Mater. **310**, c610 (2007).

[35] S. Bordács, D. Varjas, I. Kézsmárki, G. Mihaly, L. Baldassarre, A. Abouelsayed, C. A. Kuntscher, K. Ohgushi, and Y. Tokura, Magnetic-Order-Induced Crystal Symmetry Lowering in ACr_2O_4 Ferrimagnetic Spinels, Phys. Rev. Lett. **103**, 077205 (2009).

[36] M. R. Suchomel, D. P. Shoemaker, L. Ribaud, M. C. Kemei, and R. Seshadri, Spin-induced symmetry breaking in orbitally ordered $NiCr_2O_4$ and $CuCr_2O_4$, Phys. Rev. B **86**, 054406 (2012).

[37] V. Kocsis, S. Bordács, D. Varjas, K. Penc, A. Abouelsayed, C. A. Kuntscher, K. Ohgushi, Y. Tokura, and I. Kézsmárki, Magnetoelasticity in ACr_2O_4 spinel oxides (A = Mn, Fe, Co, Ni, and Cu), Phys. Rev. B **87**, 064416 (2013).

[38] C. Dejoie, M. Coduri, S. Petitdemange, C. Giacobbe, E. Covacci, O. Grimaldi, P. O. Autran, M. W. Mogodi, D. Ś. Jung, and A. N. Fitch, Combining a nine-crystal multi-analyser stage with a two-dimensional detector for high-resolution powder x-ray diffraction, J. Appl. Crystallogr. **51**, 1721 (2018).

[39] D. M. Evans and O. G. Grendal, Determining Symmetry and Structure of $FeCr_2S_4$. European Synchrotron Radiation Facility (ESRF) (2021), doi: 10.15151/ESRF-ES-472484909

[40] M. I. Aroyo, J. M. Perez-Mato, D. Orobengoa, E. Tasci, G. De La Flor, and A. Kirov, Crystallography online: Bilbao crystallographic server, Bulg. Chem. Commun. **43**, 183 (2011).

[41] R. Küchler, A. Wörl, and P. Gegenwart, M. Berben, B. Bryant, and S. Wiedmann, The world's smallest capacitive dilatometer, for high-resolution thermal expansion and magnetostriction in high magnetic fields, Rev. Sci. Instr. **88**, 083903 (2017).

[42] R. Küchler, T. Bauer, M. Brando, and F. Steglich, A compact and miniaturized high resolution capacitance dilatometer for measuring thermal expansion and magnetostriction, Rev. Sci. Instr. **83**, 095102 (2012).

[43] K. Momma and F. Izumi, VESTA 3 for three-dimensional visualization of crystal, volumetric and morphology data, J. Appl. Crystallogr. **44**, 1272 (2011).